Spatially patterned light amplification without inversion

Hamid R. Hamedi [a],*, Vassilios Yannopapas [b], Emmanuel Paspalakis [c], Julius Ruseckas [a]

[a] Baltic Institute of Advanced Technology, Pilies St. 16-8, LT-01403 Vilnius, Lithuania
[b] Department of Physics, School of Applied Mathematical and Physical Sciences, National Technical University of Athens, Athens 157 80, Greece
[c] Materials Science Department, School of Natural Sciences, University of Patras, Patras 265 04, Greece

ARTICLE INFO

ABSTRACT

In this paper a method is proposed for achieving spatially dependent amplification without inversion (AWI) by exposing a quantum emitter to two weak probe beams carrying orbital angular momentum. The emitter has a double-V level scheme consisting of four energy levels in two interlinked V subsystems and possesses a closely spaced doublet of upper energy levels. Depending on the initial state, the system exhibits spatially patterned AWI, optical transparency, and light amplification with population inversion, which are contingent on the presence of quantum interference in spontaneous emission from the doublet. In a scenario when the emitter is positioned in proximity to a plasmonic nanostructure, the degree of AWI can be controlled by adjusting the metasurface-emitter separation. This allows precise control over light–matter interactions at the nanoscale and can lead to advanced quantum photonic devices.

Introduction

In the realm of quantum optics and laser physics, the introduction of coherence to multilevel quantum systems can lead to a variety of unexpected effects in the interactions between light and matter [1–8]. Notably, coherence in multilevel atomic systems enables the generation of coherent radiation through quantum interference, resulting in new kinds of coherent radiation sources without the need for population inversion. This is known as amplification or lasing without inversion (referred to as AWI, LWI), a well-established concept in laser physics [9–17].

In addition to its polarization and intensity, light can also carry orbital angular momentum (OAM) [18,19] which can take on any integer value. This property of light arises from the spatial variation of the phase of its wavefront, which can be associated with a rotation of the beam around its propagation axis. The associated wavefronts are described as having a helical shape, and the beams are often referred to as "vortex beams". The orbital angular momentum of a vortex beam has led to many interesting applications in fields such as quantum communication, microscopy, and optical trapping. One particularly fascinating aspect of OAM is the ability to encode information in the different values of OAM. By manipulating the OAM of light, it is possible to create multiple channels for transmitting information, which can increase the bandwidth and capacity of optical communication systems.

Optical vortex beams interacting with quantum systems offer a range of intriguing effects. These effects include light-induced torque [20,21], atom vortex beams [22], entanglement of orbital angular momentum (OAM) states of photon pairs [23,24], OAM-based four-wave mixing [25,26], creation of an atomic compass [27], mechanical impacts of OAM on particles and atoms [28], and rotation of particles in optical tweezers [29,30]. Additionally, vortex slow light [31–33] can be used to provide further prospects for manipulating optical information during the storage and retrieval of slow light. Twisted slow light also offers additional possibilities for optical manipulation [34,35].

In this paper, we propose an approach to achieve spatially dependent AWI by utilizing weak probe beams with azimuthally varying polarization and phase structures interacting with a quantum emitter (QE). While prior research has shown that atoms can interact with phase-structured light to create spatially dependent electromagnetically induced transparency (EIT), as evidenced in Refs. [36–38], our approach generates a spatially structured amplification effect (with or without population inversion).

The underlying principle of our method of spatially varying AWI is rooted in the phenomenon of quantum interference (QI) between spontaneous emission channels. Although the three-level V model scheme is frequently cited in the literature as an illustration of QI in spontaneous emission [1,6,39–45], this study delves into a more intricate light–matter coupling, which takes the form of a double-V scheme. Such a

system is composed of four energy levels, which are interconnected to form two subsystems, each in a V-type configuration. We have recently utilized this level scheme to study induced enhanced torque via quantum interference in spontaneous emission [46].

The V-type QE exhibits QI in spontaneous emission only when two closely spaced upper levels decay to a common lower level [39,40], with nonorthogonal electric dipoles that maximize interference when oriented almost parallel or anti-parallel. However, perfect QI is not achievable if each leg of the V-model interacts with a separate coupling field [40], as the Rabi frequencies of laser fields coupling each transition are linked to the alignment of the two matrix elements, leading to a reduction of Rabi frequencies to zero in the case of perfect QI. In contrast, the four-level double-V light–matter coupling scheme allows for perfect interference with individual coupling. This system involves two upper and two lower states, with the two excited states connected to a third lower level using two laser beams, while they decay to a fourth lower level, allowing for interference in the corresponding spontaneous emission channels.

In the first step of our study, we examine the spatially structured effects that arise from the QI of spontaneous emission from the doublet. Depending on the initial state of the QEs, we observe spatially dependent optical transparency, amplification of light with population inversion, as well as AWI due to QI. However, in typical emitters, the dipole matrix elements are orthogonal, making QI in spontaneous emission challenging to achieve. Nonetheless, Agarwal demonstrated that QI can be induced by placing the QE in close proximity to a photonic structure that creates an anisotropic Purcell effect. This effect strongly (ideally completely) suppresses the decay rate for one of the two possible dipole orientations, while retaining the decay rate for the second orientation [42]. Expanding on this understanding and building upon the insights gained in the first step, we proceed to the second step of our study, which investigates how the presence of a plasmonic nanostructure induces spatially dependent petal-like AWI patterns with $2l$- fold symmetry. The level of light amplification can be remotely controlled by adjusting the distance from the nanostructure. This allows for precise manipulation of the spatially dependent AWI structures, opening up new avenues for applications in quantum information and communication technologies.

It should be pointed out that our recent research focused on the effects of optical transparency and nonlinearity in a quantum system situated adjacent to a plasmonic nanostructure [47]. Specifically, we investigated the impact of a single vortex probe beam on the system. We have also proposed a method to detect structured light through measuring the absorption profile of a non-vortex probe beam in a highly resonant five-level atom–light coupling setup [37]. In both studies, a weak non-vortex probe beam was used to identify areas of spatially dependent optical transparency and nonlinearity induced by other optical beams carrying OAM. However, our current research takes a different approach and objective. Our goal is to measure the amplification of structured light in quantum systems, both in free-space and near plasmonic nanostructures, and observe regions of light amplification without population inversion. In this study, the azimuthal modulation of the amplification profile is determined by the phase and polarization of the weak vortex probe fields themselves. This approach is distinct from previous studies that required a nonvortex beam to detect spatially dependent effects. Moreover, it is simpler to implement experimentally, as it only requires one type of probe beam (with OAM) interacting with the quantum system [36].

Spatially dependent AWI may offer potential applications in the development of compact and efficient laser sources. By selectively amplifying certain regions of a laser medium, it may be possible to develop laser sources with higher output powers and efficiencies than traditional laser sources, making them useful in a variety of fields such as materials processing, laser micromachining, and laser-based spectroscopy. Additionally, spatially dependent AWI could be potentially important in the development of ultrafast optical switches, filters, and
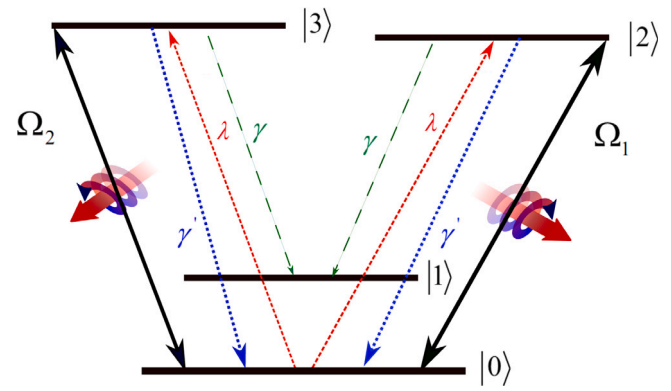

Fig. 1. The level structure of a quantum emitter (QE) in double-V configuration consists of two lower states $|0\rangle$ and $|1\rangle$ and two excited levels $|2\rangle$ and $|3\rangle$ that are closely spaced. This configuration can be realized in a variety of systems, such as atoms, molecules, or quantum dots. To excite the system, a pair of weak and spatially inhomogeneous probe vortex beams, denoted as Ω_1 and Ω_2 are employed.

modulators. By using spatially patterned AWI to selectively control the propagation of optical pulses, it may be possible to develop optical switches and modulators that operate on ultrafast timescales, which could be useful in high-speed communication and signal processing applications.

Theoretical framework and methods

Modeling light–matter interaction

Let us consider a basic model of a quantum emitter (QE) in a double-V configuration, consisting of two lower states $|0\rangle$ and $|1\rangle$ and a pair of closely spaced upper states $|2\rangle$ and $|3\rangle$. Such a model can be used to describe a variety of systems, such as atoms, molecules, or quantum dots, with the corresponding level diagram shown in Fig. 1. The excited levels $|2\rangle$ and $|3\rangle$ decay to the lower states $|1\rangle$ and $|0\rangle$ with rates $\gamma_{21}, \gamma_{31} (\gamma_{21} = \gamma_{31} = \gamma)$ and $\gamma'_{21}, \gamma'_{31}$ $(\gamma'_{21} = \gamma'_{31} = \gamma')$, respectively. The QE is also subject to incoherent pumping by two fields, λ_1 and λ_2 $(\lambda_1 = \lambda_2 = \lambda)$ which transfer populations from the lower state $|0\rangle$ to excited states $|2\rangle$ and $|3\rangle$, thus acting as a one-way pump process. The lower states are coupled to the set of upper states by a pair of probe laser fields Ω_1 and Ω_2 which are weak and spatially inhomogeneous.

The interaction between matter and light in the double-V model quantum emitter is described by the Hamiltonian H in the interaction representation. This Hamiltonian can be expressed as:

$$H = \hbar \left(-\delta - \frac{\omega_{32}}{2} \right) |2\rangle\langle2| + \hbar \left(-\delta + \frac{\omega_{32}}{2} \right) |3\rangle\langle3|$$
$$- \left(\hbar\Omega_1 |0\rangle\langle2| + \hbar\Omega_2 |0\rangle\langle3| + \text{H.c.} \right). \tag{1}$$

Here, δ represents the detuning from resonance with the average transition energies of upper states $|2\rangle$ and $|3\rangle$ from state $|0\rangle$. The detuning is calculated as $\delta = \omega - \tilde{\omega}$, where $\tilde{\omega} = (\omega_2 + \omega_3)/2 - \omega_0$. The energy splitting between the excited sublevels is represented by $\omega_{32} = (\omega_3 - \omega_2)/2$, and ω denotes the angular frequency of the fields (assuming equal frequencies for both fields). The energy of state $|i\rangle$ is represented by $\hbar\omega_i$, where i ranges from 0 to 3. The Hamiltonian includes terms for both the probe fields and their Hermitian conjugates, denoted by H.c.

Assuming that two vortex beams, denoted by Ω_1 and Ω_2, are interacting with two legs of the lower V subsystem in the four-level double-V model QE (as shown in Fig. 1), we can express them as follows:

$$\Omega_1 = |\Omega_1| \left(\frac{r}{w} \right)^{|l|} e^{-r^2/w^2} e^{il\phi}, \tag{2}$$

$$\Omega_2 = |\Omega_2| \left(\frac{r}{w} \right)^{|l|} e^{-r^2/w^2} e^{-il\phi}. \tag{3}$$

$$\rho_{20} = \frac{i\Omega_2\kappa(\rho_{33}-\rho_{00}) + i\Omega_1(i\delta - \frac{i\omega_{32}}{2} - \gamma - \gamma' - \lambda)(\rho_{22}-\rho_{00}) + i\Omega_1\kappa\rho_{32} + i\Omega_2(i\delta - \frac{i\omega_{32}}{2} - \gamma - \gamma' - \lambda)\rho_{23}}{(i\delta + \frac{i\omega_{32}}{2} - \gamma - \gamma' - \lambda)(i\delta - \frac{i\omega_{32}}{2} - \gamma - \gamma' - \lambda) - \kappa^2}, \tag{10}$$

$$\rho_{30} = \frac{i\Omega_1\kappa(\rho_{22}-\rho_{00}) + i\Omega_2(\delta + \frac{i\omega_{32}}{2} - \gamma - \gamma' - \lambda)(\rho_{33}-\rho_{00}) + i\Omega_2\kappa\rho_{23} + i\Omega_1(\delta + \frac{i\omega_{32}}{2} - \gamma - \gamma' - \lambda)\rho_{32}}{(i\delta + \frac{i\omega_{32}}{2} - \gamma - \gamma' - \lambda)(i\delta - \frac{i\omega_{32}}{2} - \gamma - \gamma' - \lambda) - \kappa^2}, \tag{11}$$

Box I.

Here, r represents the cylindrical radius, l is an integer that represent the topological (OAM) number, ϕ denotes the azimuthal angle, w represents the beam waist, and $|\Omega_1|$ and $|\Omega_2|$ represent the strength of the position-dependent vortex beams.

Steady-state matter wave equations: Solutions and analysis

We can gain insight into the behavior of the population and coherence dynamics by applying the Liouville equation of motion for the density matrix, based on Eq. (1). The Weisskopf–Wigner theory of spontaneous emission [48] can then be utilized to derive the following equations [39,40,49]

$$\dot{\rho}_{20} = (i\delta + \frac{i\omega_{32}}{2} - \gamma - \gamma' - \lambda)\rho_{20} + i\Omega_1(\rho_{00} - \rho_{22}) - i\Omega_2\rho_{23} - \kappa\rho_{30}, \tag{4}$$

$$\dot{\rho}_{30} = (i\delta - \frac{i\omega_{32}}{2} - \gamma - \gamma' - \lambda)\rho_{30} + i\Omega_2(\rho_{00} - \rho_{33}) - i\Omega_1\rho_{32} - \kappa\rho_{20}, \tag{5}$$

$$\dot{\rho}_{23} = (i\omega_{32} - 2\gamma - 2\gamma')\rho_{23} + i\Omega_1\rho_{03} - i\Omega_2\rho_{20} - \kappa(\rho_{22} + \rho_{33}), \tag{6}$$

$$\dot{\rho}_{22} = -2(\gamma + \gamma')\rho_{22} + \lambda\rho_{00} + i\Omega_1(\rho_{02} - \rho_{20}) - \kappa(\rho_{23} + \rho_{32}), \tag{7}$$

$$\dot{\rho}_{33} = -2(\gamma + \gamma')\rho_{33} + \lambda\rho_{00} + i\Omega_2(\rho_{03} - \rho_{30}) - \kappa(\rho_{23} + \rho_{32}), \tag{8}$$

$$\dot{\rho}_{00} = 2\gamma'(\rho_{22} + \rho_{33}) - 2\lambda\rho_{00} - i\Omega_1(\rho_{02} - \rho_{20}) - i\Omega_2(\rho_{03} - \rho_{30}). \tag{9}$$

These equations are subject to two constraints: first, the elements of the density matrix, denoted as ρ_{ij}, must satisfy the condition $\rho_{ij} = \rho_{ji}^*$; and second, the sum of the diagonal elements ρ_{11}, ρ_{22}, and ρ_{33} must equal one.

The above equations introduce the parameter κ, which is defined as $\kappa = p\sqrt{\gamma_{21}\gamma_{31}}$. When the decay rates from the upper levels $|2\rangle$ and $|3\rangle$ are equal, that is, $\gamma_{21} = \gamma_{31} = \gamma$, then κ simplifies to $\kappa = p\gamma$. This parameter is a measure of quantum interference (QI) resulting from spontaneous emission. The parameter p describes the degree of QI and characterizes the alignment of the two transition dipole moments, denoted as $\vec{\mu}_{21}$ and $\vec{\mu}_{31}$. Specifically, p is defined as $p = \vec{\mu}_{21}\cdot\vec{\mu}_{31}/|\vec{\mu}_{21}\|\vec{\mu}_{31}| = \cos\theta$, where θ is the angle between the two dipole moments. QI plays a crucial role in generating coherence [39,40]. The value of κ depends strongly on the orientation of the dipole polarizations. When they are nearly parallel, $\kappa \to \gamma$ ($p \to 1$), resulting in maximal interference; however, when they are perpendicular, $\kappa = 0$ and the QI effect vanishes.

Assuming a steady-state condition, the solutions for the off-diagonal density matrix elements ρ_{20} and ρ_{30} can be obtained from Eqs. (4)–(9), see Eqs. (10) and (11) given in Box I, where

$$\rho_{23} = \rho_{32}^* = \frac{\kappa(\rho_{22} + \rho_{33})}{i\omega_{32} - 2(\gamma + \gamma')}. \tag{12}$$

The Eqs. (10) and (11) are composed of two components. The initial two terms in each equation arise from the direct transitions of $|1\rangle \to |2\rangle$, $|1\rangle \to |3\rangle$, and are dependent on the population inversions $(\rho_{ii} - \rho_{11})$ (where $i = 2,3$). The latter two terms are a result of the emergence of QI, which is proportionate to the coherence terms ρ_{32} and ρ_{23}.

In this paper, we are also concerned with the absorption characteristics of the system. The imaginary part of the electric susceptibility corresponds to the absorption/gain in the medium, which can be expressed as:

$$\chi(\delta) = \frac{2N|\vec{\mu}|^2}{\varepsilon_0\hbar}\left(\frac{\rho_{20}}{\Omega_1} + \frac{\rho_{30}}{\Omega_2}\right). \tag{13}$$

Here, we have assumed that $|\vec{\mu}_{21}| = |\vec{\mu}_{31}| = |\vec{\mu}|$, where ε_0 represents the vacuum permittivity and N is the density of the quantum emitters.

When the light–matter interaction is weak, the zero-order solution of Ω_1 and Ω_2 can be obtained as

$$\rho_{22} = \rho_{33} = \frac{2\lambda(\gamma + \gamma')\left[4(\gamma + \gamma')^2 + \omega_{32}^2\right]}{-16\kappa^2(\gamma + \gamma')^2 + 4\left[4(\gamma + \gamma')^2 + \omega_{32}^2\right]\left[(\gamma + \gamma')^2 + \lambda(\gamma + \gamma')\right]}, \tag{14}$$

$$\rho_{00} = \frac{-16\kappa^2(\gamma + \gamma')^2 + 4(\gamma + \gamma')^2\left[4(\gamma + \gamma')^2 + \omega_{32}^2\right]}{-16\kappa^2(\gamma + \gamma')^2 + 4\left[4(\gamma + \gamma')^2 + \omega_{32}^2\right]\left[(\gamma + \gamma')^2 + \lambda(\gamma + \gamma')\right]}, \tag{15}$$

$$\rho_{23} = \frac{-4\lambda\kappa(\gamma + \gamma')(i\omega_{32} + 2\gamma + 2\gamma')}{-16\kappa^2(\gamma + \gamma')^2 + 4\left[4(\gamma + \gamma')^2 + \omega_{32}^2\right]\left[(\gamma + \gamma')^2 + \lambda(\gamma + \gamma')\right]}. \tag{16}$$

$$\rho_{11} = 1 - \rho_{00} - \rho_{22} - \rho_{33}. \tag{17}$$

Results and discussion

Spatially structured amplification induced by QI

The relationship between electric susceptibility (and consequently, the probe absorption that is linked to the imaginary part of susceptibility), and the presence of QI can be described using Eq. (13), in conjunction with Eqs. (10), (2) and (3). Specifically, when the QI parameter κ is present, the probe absorption/amplification displays spatial dependence. Furthermore, the dependence of steady-state solutions on the initial state of the QE can be demonstrated through the use of Eqs. (13), (10), (11), (14)–(17). This dependence is attributed to the QI term κ.

In what follows, we will examine different scenarios involving the initial states of the QE. Assuming that the upper levels $|2\rangle$ and $|3\rangle$ are degenerate ($\omega_{32} = 0$), and that the incoherent pump r is present in the system ($\lambda \neq 0$), while the free-space spontaneous decay rate is absent ($\gamma' = 0$), we can consider a perfect interference, with $\kappa = \gamma$ ($p = 1$). In such a situation, Eqs. (14)–(16) can easily be used to derive the following:

$$\rho_{00} = 0, \qquad \rho_{22} = \rho_{33} = \frac{1}{2}, \qquad \rho_{23} = -\frac{1}{2}. \tag{18}$$

This indicates that the QE is initially in an antisymmetric state $|D\rangle = \frac{|2\rangle - |3\rangle}{\sqrt{2}}$. The electric susceptibility can then be determined by substituting Eq. (18) into Eqs. (10),(11) and (13), which leads to

$$\chi(\delta) = \frac{2N|\vec{\mu}|^2}{\varepsilon_0\hbar}\frac{i}{2(i\delta - \lambda)}\left(\frac{\Omega_1 - \Omega_2}{\Omega_1} + \frac{\Omega_2 - \Omega_1}{\Omega_2}\right). \tag{19}$$

By utilizing the equations for the vortex beams defined by (2) and (3) and substituting them into Eq. (19), one can then obtain an analytical expression for the absorption/amplification of the probe field by taking the imaginary part of the equation, resulting

$$\text{Im}[\chi(\delta)] = \frac{2N|\vec{\mu}|^2}{\varepsilon_0\hbar}\left(\frac{\delta N_1 - M_1\lambda}{2\lambda^2 + 2\delta^2}\right), \tag{20}$$

where $M_1 = 2 - (X + Y)\cos(2l\phi)$, $N_1 = (X - Y)\sin(2l\phi)$, $X = \frac{|\Omega_2|}{|\Omega_1|}$ and $Y = \frac{|\Omega_1|}{|\Omega_2|}$.
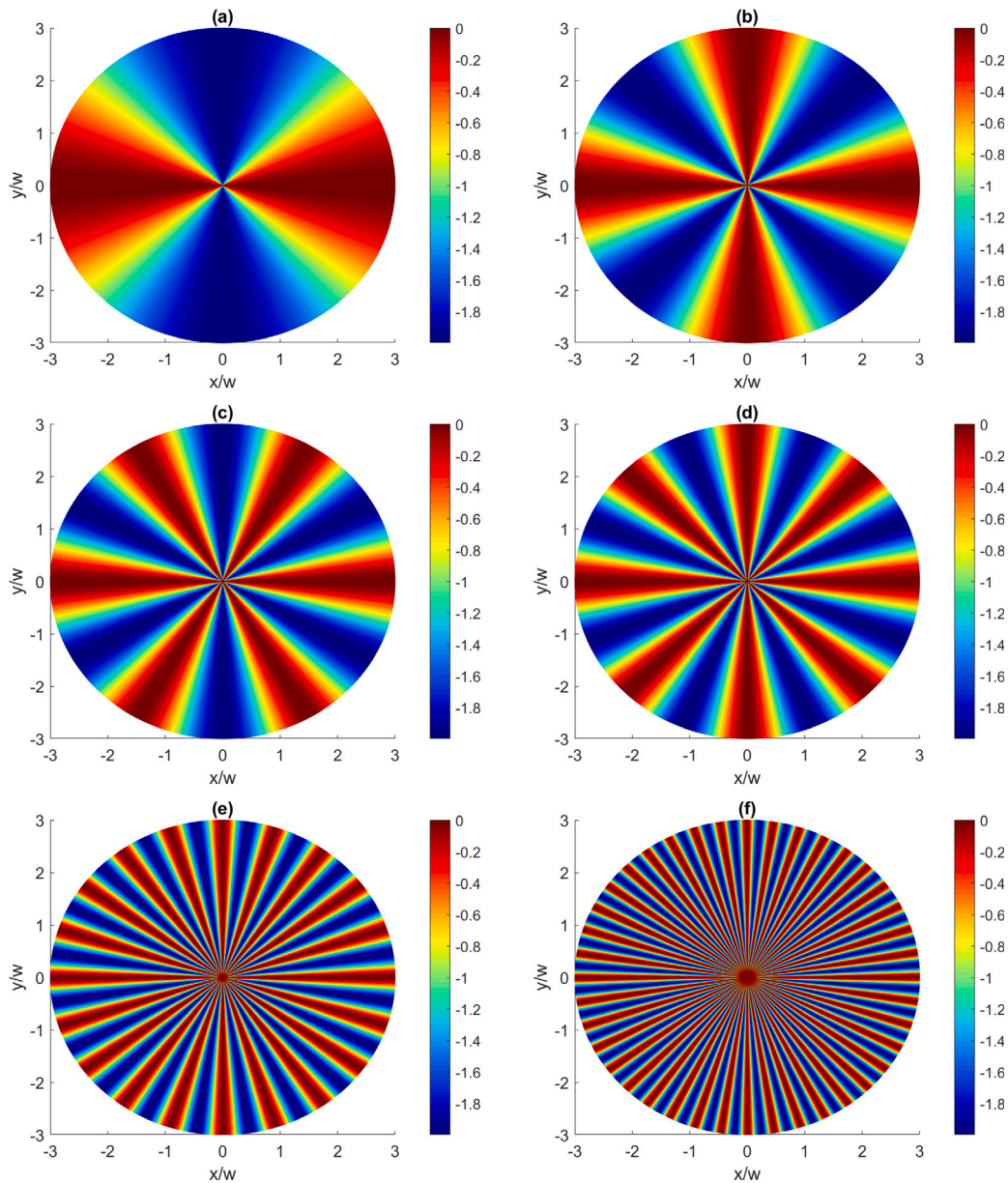
Fig. 2. Spatially dependent absorption (gain) spectrum Im(χ) (in units of $\frac{2N|\vec{\mu}|^2}{\varepsilon_0 \hbar}$) (b) for (a) $l = 1$, (b) $l = 2$, (c) $l = 3$, (d) $l = 4$, (e) $l = 10$, (f) $l = 20$. Here, $\delta = 0$, $\gamma' = 0$, $\omega_{32} = 0$, $\lambda = \gamma$, $p = 1$ (or $\kappa = \gamma$), and $|\Omega_1| = |\Omega_2| = 0.1\gamma$.

On resonance when the probe field has a frequency offset of $\delta = 0$, and the Rabi frequencies of the two driving fields are equal $|\Omega_1| = |\Omega_2| = |\Omega|$, Eq. (20) can be further simplified to

$$\text{Im}[\chi(\delta = 0)] = \frac{2N|\vec{\mu}|^2}{\varepsilon_0 \hbar} \left(\frac{\cos(2l\phi) - 1}{\lambda} \right). \qquad (21)$$

This equation reveals that the response of the medium to the probe field is azimuthally varying through azimuthal phase $\phi = \tan^{-1}(y/x)$. Specifically, the medium becomes transparent (Im[$\chi(\delta = 0)$] = 0) when $l\phi = n\pi$, where n is any integer, as the imaginary part of the susceptibility equals zero. On the other hand, the medium amplifies and lases (Im[$\chi(\delta = 0)$] < 0) for other spatial regions ($l\phi \neq n\pi$) where the imaginary part of the susceptibility is negative. The spatially structured profile displays a $2l$-fold symmetry, with transparency/gain regions distributed alternately throughout. This symmetry arises due to the spatial distribution of spatially engineered transparency regions in the medium, where the imaginary part of the susceptibility is suppressed. The formation of these regions is a result of QI in spontaneous emission,

which cancels out the imaginary part of the susceptibility at specific spatial locations, resulting in transparency. At other specific locations, the interference instead amplifies the probe beam, resulting in lasing. Such light amplification is accompanied by the population inversion in the entire 2D azimuthal space, as indicated by Eq. (18). This can be observed in Fig. 2 where we present spatially structured transparency and gain for different values of OAM number l. Our results demonstrate a petal-like pattern in the spatial distribution of the imaginary part of probe susceptibility, with each petal corresponding to a region of transparency, and the spaces between the petals corresponding to regions of spatially patterned light amplification. The number of petals observed in the spatial distribution is directly proportional to the OAM number, with each increment of the OAM number corresponding to an additional pair of petals. This provides a straightforward method for detecting structured light, simply by counting the number of pairs of petals.

Next, suppose we have the QE with nondegenerate upper levels ($\omega_{32} \neq 0$) but with no incoherent pump ($\lambda = 0$). In addition, we assume
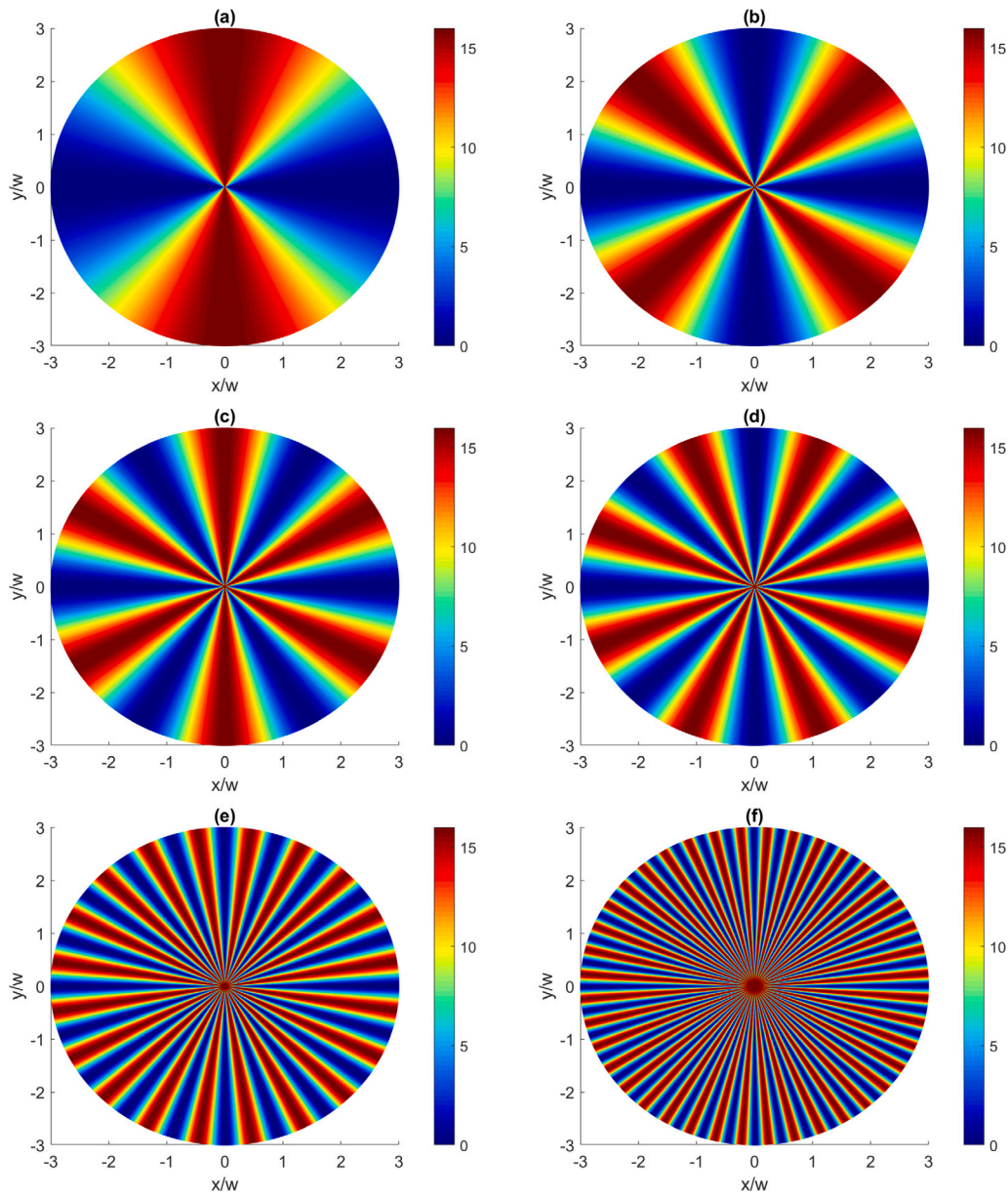
Fig. 3. Spatially dependent absorption (gain) spectrum Im(χ) (in units of $\frac{2N|\vec{\mu}|^2}{\varepsilon_0 \hbar}$) (b) for (a) $l = 1$, (b) $l = 2$, (c) $l = 3$, (d) $l = 4$, (e) $l = 10$, (f) $l = 20$. Here, $\delta = 0$, $\gamma' = 0$, $\omega_{32} = \gamma$, $\lambda = 0$, $p = 1$ (or $\kappa = \gamma$), and $|\Omega_1| = |\Omega_2| = 0.1\gamma$.

that QI is perfect ($p = 1$, which implies $\kappa = \gamma$). Under these conditions, the steady-state solutions (14)–(16) simplify to:

$$\rho_{00} = 1, \qquad \rho_{22} = \rho_{33} = 0, \qquad \rho_{23} = 0. \qquad (22)$$

This situation corresponds to the QE being in the ground state $|0\rangle$, or in the symmetric state $|B\rangle = \frac{|2\rangle + |3\rangle}{\sqrt{2}}$. It is worth noting that Eq. (22) is valid for any value of p whether perfect ($p = 1$) or imperfect ($p \neq 1$) QI. Assuming now the initial state of the QE is given by Eq. (22), we can apply it to Eqs. (10), (11) to modify the electric susceptibility (13) to

$$\chi(\delta) = \frac{2N|\vec{\mu}|^2}{\varepsilon_0 \hbar} \frac{-i\kappa(\frac{\Omega_2}{\Omega_1} + \frac{\Omega_1}{\Omega_2}) + 2i\gamma + 2\delta}{A - 2i\gamma\delta}, \qquad (23)$$

where $A = \gamma^2 + \frac{\omega_{32}^2}{4} - \kappa^2 - \delta^2$. Using the definition of optical vortices in Eqs. (2) and (3), the probe absorption can be expressed now as:

$$\text{Im}[\chi(\delta)] = \frac{2N|\vec{\mu}|^2}{\varepsilon_0 \hbar} \frac{AM_2 + 2\gamma\delta N_2}{A^2 + 4\gamma^2\delta^2}, \qquad (24)$$

with $M_2 = 2\gamma - \kappa(X + Y)\cos(2l\phi)$ and $N_2 = 2\delta + \kappa(Y - X)\sin(2l\phi)$ ($X = \frac{|\Omega_2|}{|\Omega_1|}$, $Y = \frac{|\Omega_1|}{|\Omega_2|}$).

If $|\Omega_1| = |\Omega_2| = |\Omega|$ (hence $X = Y$) is satisfied, and the detuning is zero ($\delta = 0$) with perfect QI ($\kappa = \gamma$), the expression for the probe absorption takes the form

$$\text{Im}[\chi(\delta = 0)] = \frac{2N|\vec{\mu}|^2}{\varepsilon_0 \hbar} \frac{8\gamma(1 - \cos(2l\phi))}{\omega_{32}^2}. \qquad (25)$$

Fig. 3 shows that while transparency occurs at $l\phi = n\pi$ as before, the medium becomes absorptive (Im$[\chi(\delta = 0)] > 0$) in other spatial regions ($l\phi \neq n\pi$) where the imaginary part of the susceptibility is positive. This is in contrast to the previous case, where the medium only lased in these spatial regions. The OAM number determines now the number of petals observed in the spatial distribution, with each petal associated with an area of absorption, separated by regions of spatially patterned transparency.

Let us now consider the case of vortex beams with unequal strengths, such as $|\Omega_1| = 0.2\gamma$ and $|\Omega_2| = 0.1\gamma$, as shown in Fig. 4,
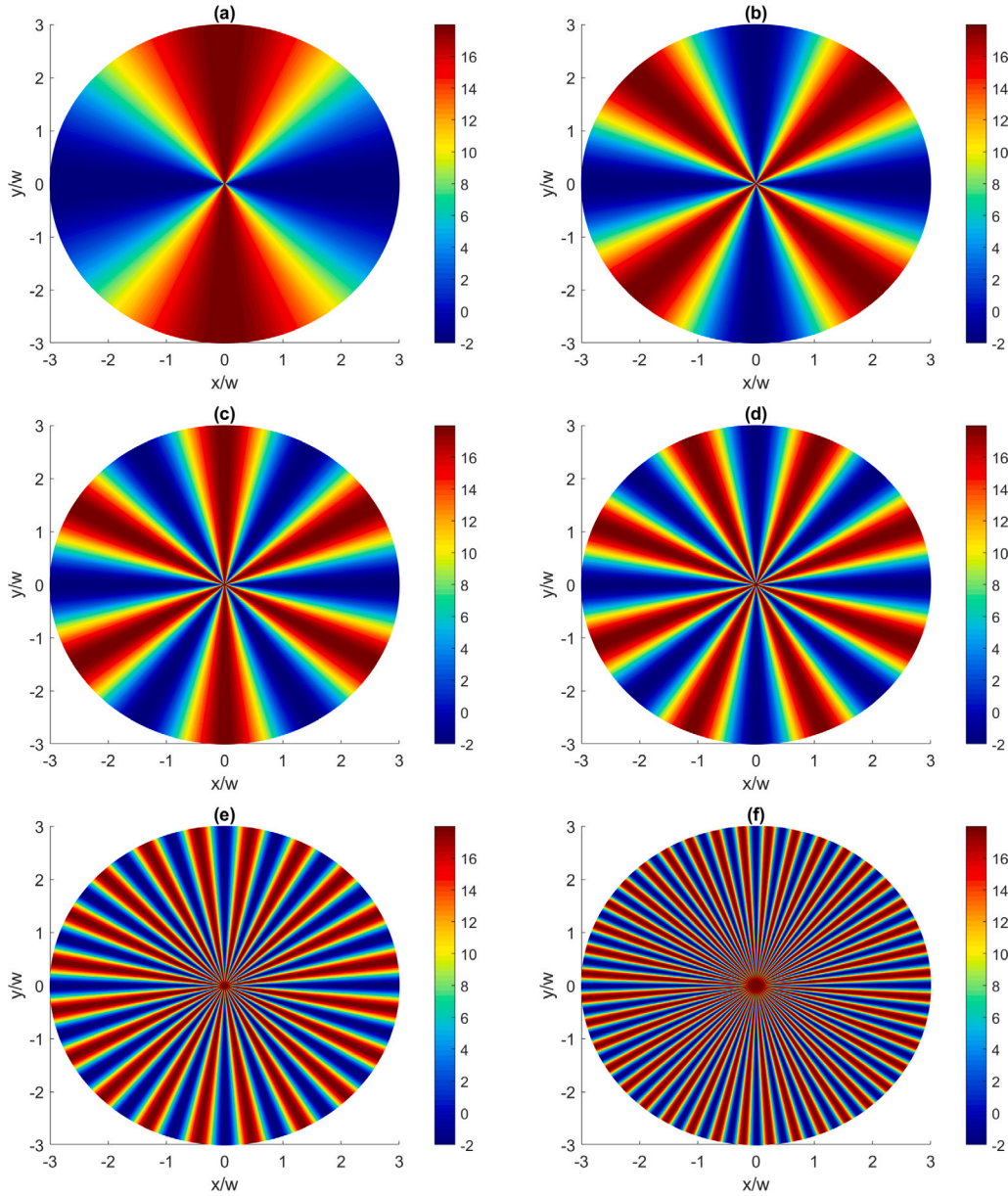
Fig. 4. Spatially dependent absorption (gain) spectrum Im(χ) (in units of $\frac{2N|\bar{\mu}|^2}{\varepsilon_0 \hbar}$) (b) for (a) $l = 1$, (b) $l = 2$, (c) $l = 3$, (d) $l = 4$, (e) $l = 10$, (f) $l = 20$. Here, $\delta = 0$, $\gamma' = 0$, $\omega_{32} = \gamma$, $\lambda = 0$, $p = 1$ (or $\kappa = \gamma$), and $|\Omega_1| = 0.2\gamma$, $|\Omega_2| = 0.1\gamma$.

while keeping $\delta = 0$ and $\kappa = \gamma$. In this scenario, Eq. (24) can convert to

$$\mathrm{Im}[\chi(\delta = 0)] = \frac{2N|\bar{\mu}|^2}{\varepsilon_0 \hbar} \frac{4\gamma \left[2 - \frac{|\Omega_1|^2 + |\Omega_2|^2}{|\Omega_1||\Omega_2|} \cos(2l\phi) \right]}{\omega_{32}^2}. \quad (26)$$

Obviously from Fig. 4, when $\cos(2l\phi)$ exceeds a certain threshold ($\cos(2l\phi) > \frac{2|\Omega_1||\Omega_2|}{|\Omega_1|^2 + |\Omega_2|^2}$), the vortex beams can stimulate the QEs in the medium to emit coherent radiation, thereby causing the medium to amplify. This type of amplification does not require a population inversion (see Eq. (22)), leading to spatially dependent AWI. However, if $\cos(2l\phi)$ falls below the threshold $\frac{2|\Omega_1||\Omega_2|}{|\Omega_1|^2 + |\Omega_2|^2}$, the medium can become either transparent ($\cos(2l\phi) = 2\frac{|\Omega_1||\Omega_2|}{|\Omega_1|^2 + |\Omega_2|^2}$) or absorb ($\cos(2l\phi) < 2\frac{|\Omega_1||\Omega_2|}{|\Omega_1|^2 + |\Omega_2|^2}$) the incident radiation, depending on the exact value of $\cos(2l\phi)$. The specific threshold value of $\cos(2l\phi)$ that distinguishes between the AMI and transparency/absorption regions depends on the relative strengths of the vortex beams. Therefore, this threshold value can vary depending

on the specific experimental setup and the properties of the medium being used.

Spatially dependent AWI implementation in plasmonic nanostructures

In the preceding section, we introduced the concept of spatially dependent amplification without inversion (AWI). Building upon that idea, we now explore a possible implementation in the case where the quantum emitter is in close proximity to a plasmonic nanostructure. Specifically, we examine how this configuration can be utilized to achieve spatially dependent AWI. By considering this scenario, we can gain insights into the potential for unlocking new possibilities in the manipulation of light and matter at the nanoscale. Note that the spatially structured lasing effects observed earlier appeared due to the QI effect when two closely spaced upper levels of the double-V-model QE, namely $|2\rangle$ and $|3\rangle$, decay to a shared level, $|1\rangle$, allowing for interference between the corresponding spontaneous emission channels. For this type of interference effect to occur, a very precise condition
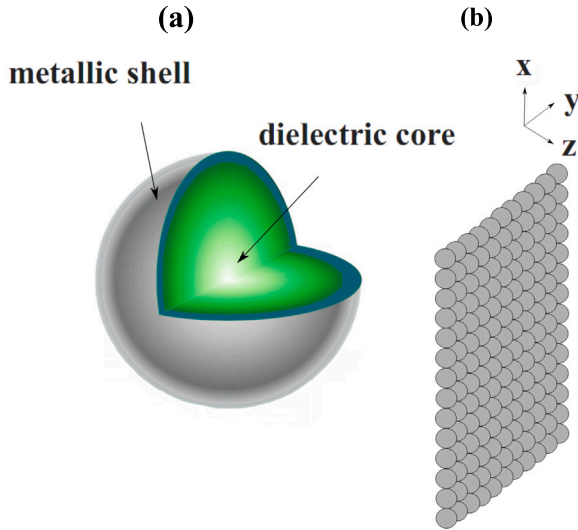
(a) (b)

metallic shell

dielectric core

Fig. 5. Panel (a) depicts a dielectric nanosphere that has been coated with metal while (b) shows a two-dimensional array of these spheres.

must be met: the dipole matrix moments of the closely spaced states $|2\rangle$ and $|3\rangle$, which decay spontaneously to the common state $|1\rangle$, must be nonorthogonal. If these matrix moments are orthogonal, QI cannot occur, presenting a challenge for common quantum systems such as atoms, molecules, and quantum dots. However, it has been suggested that an anisotropic quantum vacuum can induce QI during the spontaneous emission process when the QEs are placed near a nanophotonic structure, as predicted by Agarwal in 2000 [42].

Based on this, we will now explore the spatially dependent amplification effect that arises from the QI when the double-V QE is positioned in close proximity to a photonic nanostructure, specifically at a distance of d above its surface. In Fig. 5, we can see a metal-coated dielectric nanosphere (panel a) and a 2D array composed of a periodic array of such spheres (panel b).

The presence of a photonic structure can alter the values of the parameters γ and κ, which can be derived using equations previously published in several studies [6,41,45,50–52]. These parameters are given by:

$$\gamma = \frac{\mu_0 \mu^2 \bar{\omega}^2}{2\hbar} \hat{\varepsilon}_- \cdot \text{Im}\mathbf{G}(\mathbf{r}, \mathbf{r}; \bar{\omega}) \cdot \hat{\varepsilon}_+, \tag{27}$$

$$\kappa = \frac{\mu_0 \mu^2 \bar{\omega}^2}{2\hbar} \hat{\varepsilon}_+ \cdot \text{Im}\mathbf{G}(\mathbf{r}, \mathbf{r}; \bar{\omega}) \cdot \hat{\varepsilon}_+. \tag{28}$$

In these equations, $\mathbf{G}(\mathbf{r}, \mathbf{r}; \bar{\omega})$ represents the dyadic electromagnetic Green's tensor, which depends on the position of the quantum emitter ($\mathbf{r}$) and the frequency ($\bar{\omega}$) given by $(\omega_3 + \omega_2)/2 - \omega_1$. The value of μ_0 corresponds to the permeability of the vacuum. By using the expressions in Eqs. (27) and (28), one can calculate the values of γ and κ as follows:

$$\gamma = \frac{\mu_0 \mu^2 \bar{\omega}^2}{2\hbar} \text{Im}\left[G_\perp(\mathbf{r}, \mathbf{r}; \bar{\omega}) + G_\parallel(\mathbf{r}, \mathbf{r}; \bar{\omega})\right] = \frac{1}{2}(\Gamma_\perp + \Gamma_\parallel), \tag{29}$$

$$\kappa = \frac{\mu_0 \mu^2 \bar{\omega}^2}{2\hbar} \text{Im}\left[G_\perp(\mathbf{r}, \mathbf{r}; \bar{\omega}) - G_\parallel(\mathbf{r}, \mathbf{r}; \bar{\omega})\right] = \frac{1}{2}(\Gamma_\perp - \Gamma_\parallel). \tag{30}$$

In this context, the symbols $\perp$ and $\parallel$ refer to dipoles that are oriented normally (along the z axis) and parallel (along the x axis), respectively, to the surface of the plasmonic material. The components of the electromagnetic Green's tensor of the surrounding plasmonic environment are denoted by $G_\perp(\mathbf{r}, \mathbf{r}; \bar{\omega}) = G_{zz}(\mathbf{r}, \mathbf{r}; \bar{\omega})$ and $G_\parallel(\mathbf{r}, \mathbf{r}; \bar{\omega}) = G_{xx}(\mathbf{r}, \mathbf{r}; \bar{\omega})$. The spontaneous emission rates for an emitter oriented normal and parallel to the surface are given by e $\Gamma_{\perp,\parallel} = \mu_0 \mu^2 \bar{\omega}^2 \text{Im}\left[G_{\perp,\parallel}(\mathbf{r}, \mathbf{r}; \bar{\omega})\right]/\hbar$.

The degree of quantum interference in spontaneous emission is represented by the parameter p, which is given by

$$p = (\Gamma_\perp - \Gamma_\parallel)/(\Gamma_\perp + \Gamma_\parallel). \tag{31}$$

When p equals 1, the maximum level of quantum interference occurs [53]. This typically happens when the emitter is in close proximity to a structure that can fully suppress $\Gamma_\perp$. On the other hand, if the emitter is situated in free-space vacuum, then $\Gamma_\perp = \Gamma_\parallel$, yielding $\kappa = 0$ and consequently $p = 0$. Therefore, quantum interference is completely absent in the double-V system.

The focus of the current study is a plasmonic nanostructure consisting of a 2D square lattice of silica nanospheres coated with gold (see Figs. 5(a) and 5(b)). The periodic arrangement of such nanospheres (nanoshells) can be achieved through various techniques, such as self-assembly [54], nanopatterning, and nanolithography [55]. The dielectric function of the gold-coated nanoshell is described by a Drude-type electric permittivity given by:

$$\epsilon(\omega) = 1 - \frac{\omega_p^2}{\omega(\omega + i/\tau)}. \tag{32}$$

Here, ω_p and τ represent the bulk plasma frequency and the relaxation time of the conduction-band electrons of the gold, respectively. The plasma frequency for gold typically has a value of $\hbar\omega_p = 8.99$ eV [56, 57]. This value is essential in determining the length scale of the system, which is approximately $c/\omega_p \approx 22$ nm. Assuming a dielectric constant of $\epsilon = 2.1$ for SiO$_2$, all subsequent calculations take into account the assumption that $\tau^{-1} = 0.05\omega_p$. Additionally, the lattice constant of the square array is determined by $a = 2c/\omega_p$. The nanoshells' geometry is described by two parameters: the total sphere radius $S = c/\omega_p$ and the core radius $S_c = 0.7c/\omega_p$.

The electromagnetic Green's tensor that provides the relevant spontaneous emission rates, $\Gamma_\perp$ and $\Gamma_\parallel$, can be expressed as [50,58,59]:

$$G_{ii'}^{EE}(\mathbf{r}, \mathbf{r}; \bar{\omega}) = g_{ii'}^{EE}(\mathbf{r}, \mathbf{r}; \omega) - \frac{i}{8\pi^2} \int\int_{SBZ} d^2\mathbf{k}_\parallel \sum_{\mathbf{g}} \frac{1}{c^2 K_{\mathbf{g};z}^+}$$
$$\times v_{\mathbf{g}\mathbf{k}_\parallel;i}(\mathbf{r}) \exp(-i\mathbf{K}_{\mathbf{g}}^+ \cdot \mathbf{r})\hat{e}_{i'}(\mathbf{K}_{\mathbf{g}}^+), \tag{33}$$

where the function $v_{\mathbf{g}\mathbf{k}_\parallel;i}(\mathbf{r})$ is defined as:

$$v_{\mathbf{g}\mathbf{k}_\parallel;i}(\mathbf{r}) = \sum_{\mathbf{g}'} R_{\mathbf{g}';\mathbf{g}}(\omega, \mathbf{k}_\parallel) \exp(-i\mathbf{K}_{\mathbf{g}'}^- \cdot \mathbf{r})\hat{e}_i(\mathbf{K}_{\mathbf{g}'}^-). \tag{34}$$

The vectors $\mathbf{g}$ are the reciprocal-lattice vectors associated with the 2D periodic lattice of the scatterer plane, while $\mathbf{k}_\parallel$ is the reduced wave vector that lies within the surface Brillouin zone of the reciprocal lattice of the spheres [60]. The vector $\mathbf{K}_{\mathbf{g}}^\pm$ is defined as:

$$\mathbf{K}_{\mathbf{g}}^\pm = \{\mathbf{k}_\parallel + \mathbf{g}, \pm [q^2 - (\mathbf{k}_\parallel + \mathbf{g})^2]^{1/2}\}. \tag{35}$$

When $q^2 = \omega^2/c^2 < (k_\parallel + \mathbf{g})^2$, the wave-vector $\mathbf{K}_{\mathbf{g}}^\pm$ acquires an imaginary part, resulting in an evanescent wave. In Eq. (33), the term $g_{ii'}^{EE}(\mathbf{r}, \mathbf{r}; \omega)$ represents the free-space Green's tensor, while $\hat{e}_i(\mathbf{K}_{\mathbf{g}}^\pm)$ denotes the polar unit vector normal to $\mathbf{K}_{\mathbf{g}}^\pm$. Additionally, the reflection matrix $R_{\mathbf{g}';\mathbf{g}}(\omega, \mathbf{k}_\parallel)$ sums over the reflected (diffracted) beams generated by the incidence of a plane wave from the left of the scatterer plane, with contributions from all $\mathbf{g}$'s. The terms corresponding to s-polarized waves, which contain components with the unit vector $\hat{e}_i(\mathbf{K}_{\mathbf{g}}^\pm)$ normal to $\mathbf{K}_{\mathbf{g}}^\pm$, make a trivial contribution to the total decay rates and are therefore neglected in Eq. (33) [60].

We set $\bar{\omega} = 0.632\omega_p$ and define d as the distance between the plasmonic nanostructure's surface (plane of sphere centers) and the quantum system. The values of $\Gamma_\perp$ and $\Gamma_\parallel$ associated with different distances to the plasmonic nanostructure used in this study are shown in Fig. 3 of Ref. [61]. The findings show that $\Gamma_\parallel$ is significantly suppressed, and its actual value is much smaller than the corresponding free-space decay rate. Additionally, the value of $\Gamma_\perp$ decreases as the distance between the quantum emitter and the plasmonic nanostructure increases. In close proximity to the lattice of the plasmonic nanoshells, $\Gamma_\perp$ becomes much larger than the free-space decay rate. For distances up to $0.6c/\omega_p$, $\Gamma_\perp$ is higher than the decay rate in vacuum. However, for separations between $0.65c/\omega_p$ and c/ω_p, the decay rate $\Gamma_\perp$ is lower than that in vacuum.
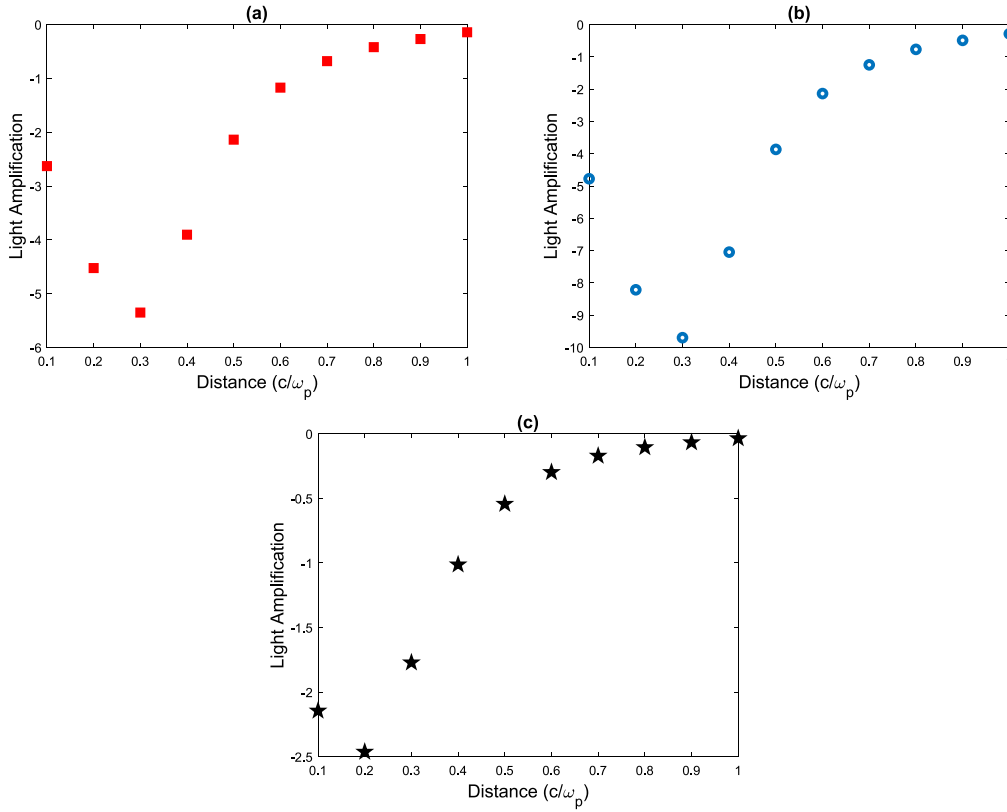
Fig. 6. (a) Scatter plot illustrating the relationship between light amplification and distance from a plasmonic nanostructure. Light amplification is measured in units of $\frac{2N|\vec{\mu}|^2}{\varepsilon_0\hbar}$, and the minimum value of the imaginary part of the susceptibility ($\mathrm{Im}(\chi)$) is used as a metric. The plot examines also how changing certain parameters, such as strengths of the vortex beams and the doublet splitting, affect the amplification-distance relationship. Three cases are shown: (a) with standard parameters $\delta = 0$, $\gamma' = 0$, $\omega_{32} = \gamma$, $\lambda = 0$, $|\Omega_1| = 0.2\gamma$, $|\Omega_2| = 0.1\gamma$ and $l = 1$, (b) with increased $|\Omega_1|$ to $|\Omega_1| = 0.25\gamma$, and (c) with increased ω_{32} to $\omega_{32} = 2\gamma$.

In order to capture the spatially varying amplification of the double-V QE near the plasmonic nanostructure, resulting from the interplay between optical vortex beams and the presence of QI in spontaneous emission, we focus on the case where ω_{32} is non-zero and λ is equal to zero. This is akin to the second scenario discussed in the previous section. It is worth noting that the first scenario, where $p = 1$ ($\kappa = \gamma$) and maximum interference is achieved, cannot occur near the plasmonic nanostructures.

The equation that describes the absorption of the probe field in this case can be obtained by substituting Eqs. (29) and (30) into Eq. (24) and setting the resonance condition $\delta = 0$. The resulting equation takes the form:

$$\mathrm{Im}[\chi(\delta = 0)]$$

$$= \frac{2N|\vec{\mu}|^2}{\varepsilon_0\hbar}\frac{4\left\{\Gamma_\perp\left[1 - \frac{|\Omega_1|^2 + |\Omega_2|^2}{2|\Omega_1||\Omega_2|}\cos(2l\phi)\right] + \Gamma_\parallel\left[1 + \frac{|\Omega_1|^2 + |\Omega_2|^2}{2|\Omega_1||\Omega_2|}\cos(2l\phi)\right]\right\}}{\omega_{32}^2 + 4\Gamma_\perp\Gamma_\parallel}.$$

(36)

This equation contains two terms in the numerator, with the first term responsible for amplification and the second term leading to absorption. However, since the decay rate perpendicular to the surface of the plasmonic nanostructure, $\Gamma_\perp$, is substantially greater than the decay rate parallel to the surface, $\Gamma_\parallel$, the first term prevails in certain spatial locations, resulting in specific regions experiencing light amplification, where the imaginary component of χ (with $\delta = 0$) turns negative. Such a gain occurs without any population inversion as provided by Eq. (22).

We do not replicate the spatially dependent plots in this section since they closely resemble those in the previous section. Instead, we use scatter plots to showcase the amplification levels and their variation with distance from a plasmonic nanostructure. Fig. 6 shows a scatter plot illustrating the relationship between AWI and distance from a plasmonic nanostructure. Light amplification is measured in units of $\frac{2N|\vec{\mu}|^2}{\varepsilon_0\hbar}$, and the minimum value of the imaginary part of the susceptibility ($\mathrm{Im}(\chi)$) is used as a metric. The plot illustrates how changing certain parameters, such as the strengths of the vortex beams and energy splitting, affect the amplification-distance relationship. Three cases are shown: (a) with standard parameters, (b) with increased $|\Omega_1|$, and (c) with increased ω_{32}. Panel (a) shows that the light amplification deepens for distances up to $d = 0.3c/\omega_p$ and then begins to decrease for distances from $0.4c/\omega_p$ to c/ω_p. In particular, the level of amplification increases with increasing $|\Omega_1|$ to $|\Omega_1| = 0.25\gamma$, as shown in panel (b). Notably, increasing ω_{32} to $\omega_{32} = 2\gamma$ actually results in less amplification, as seen in panel (c). However, the largest gain is now attained at a distance of $d = 0.2c/\omega_p$. The results of the study suggest that the amplification of light can be controlled remotely by adjusting system parameters. It is worth noting that we have only investigated here the case where the strengths of the vortex beams are unequal, i.e., $|\Omega_1| \neq |\Omega_2|$. In the event that $|\Omega_1| = |\Omega_2|$, no amplification will occur. Instead, spatially dependent absorption/transparency structures with $2l$-fold symmetry will be produced, similar to those illustrated in Fig. 3.

The probe laser fields Ω_1 and Ω_2 can be created by passing a linearly polarized probe laser through a q plate (liquid-crystal-based retardation wave plates with an inhomogeneous optical axis, which exhibit an azimuthal topological charge q) with $q = l/2$, similarly as in Ref. [36]. In this case, the resulting light will have correlated circular polarization and angular momentum. Left and right circularly polarized components couple to the sublevels with magnetic quantum numbers $m_F = \pm 1$. Each polarization component exhibits a uniform intensity in the azimuthal direction, featuring a dark vortex core at its center. As the orthogonal polarizations do not interfere with each other, the overall beam maintains its uniform azimuthal intensity.

Concluding remarks

To summarize, this study investigates the interaction between a double-V-model QE and weak probe beams carrying OAM. By taking into account QI in spontaneous emission from the doublet of upper energy levels, the study reveals the emergence of both spatially dependent transparency and amplification with or without population inversion, depending on the initial state of the QEs. When placing the QE next to a plasmonic nanostructure, the distance between the QE and a nanostructure can be controlled to create spatially structured AWI patterns, opening new avenues for manipulating such optical effects. The ability to manipulate the spatially dependent lasing through the topological charge and proximity to a plasmonic nanostructure may lead to breakthroughs in optical information processing, optical communication, and sensing, improve our understanding of quantum emitter–environment interactions and highlight the potential for achieving precise control over light–matter interactions at the nanoscale.

The double-V-model QE setup can be experimentally implemented using various atomic schemes, such as those with two $J = 0$ states for the lower states ($|0\rangle$ and $|1\rangle$), and $M = \pm 1$ sublevels of a $J = 1$ state for the excited states ($|2\rangle$ and $|3\rangle$). By applying a static magnetic field, the energy difference $\hbar\omega_{32}$ can be adjusted. Another possible implementation is using hyperfine sublevels of the D lines in alkali-metal atoms such as ^{85}Rb and ^{87}Rb [62–64]. Alternatively, a dual CdSe/ZnS/CdSe quantum dot system can also be utilized [62].

CRediT authorship contribution statement

Hamid R. Hamedi: Formal analysis, Investigation, Methodology, Writing – original draft, Writing – review & editing. **Vassilios Yannopapas:** Validation, Writing – review & editing. **Emmanuel Paspalakis:** Supervision, Validation, Writing – review & editing. **Julius Ruseckas:** Methodology, Supervision, Validation, Writing – review & editing.

Declaration of competing interest

The authors declare that they have no known competing financial interests or personal relationships that could have appeared to influence the work reported in this paper.

Data availability

Data will be made available on request.

Acknowledgment

References

[1] Scully MO, Zhu S-Y, Gavrielides A. Degenerate quantum-beat laser: Lasing without inversion and inversion without lasing. Phys Rev Lett 1989;62:2813.

[2] Harris SE. Electromagnetically induced transparency. Phys Today 1997;50:36.

[3] Heckenberg NR, McDuff R, Smith CP, White AG. Generation of optical phase singularities by computer-generated holograms. Opt Lett 1992;17:221.

[4] Hamedi HR, Yannopapas V, Juzeliūas G, Paspalakis E. Coherent optical effects in a three-level quantum emitter near a periodic plasmonic nanostructure. Phys Rev B 2022;106:035419.

[5] Vitanov NV, Rangelov AA, Shore BW, Bergmann K. Stimulated raman adiabatic passage in physics, chemistry, and beyond. Rev Modern Phys 2017;89:015006.

[6] Yang Y, Xu J, Chen H, Zhu S. Quantum interference enhancement with left-handed materials. Phys Rev Lett 2008;100:043601.

[7] Zibrov AS, Matsko AB, Kocharovskaya O, Rostovtsev YV, Welch GR, Scully MO. Transporting and time reversing light via atomic coherence. Phys Rev Lett 2002;88:103601.

[8] Fleischhauer M, Imamoglu A, Marangos JP. Electromagnetically induced transparency: Optics in coherent media. Rev Modern Phys 2005;77:633.

[9] Mompart J, Corbalan R. Lasing without inversion. J Opt B: Quantum Semiclass Opt 2000;2:R7.

[10] Kocharovskaya O. Amplification and lasing without inversion. Phys Rep 1992;219:175.

[11] Zhu Y. Lasing without inversion in a closed three-level system. Phys Rev A 1992;45:R6149.

[12] Richter M, Lytova M, Morales F, Haessler S, Smirnova O, Spanner M, et al. Rotational quantum beat lasing without inversion. Optica 2020;7:586.

[13] Svidzinsky AA, Yuan L, Scully MO. Transient lasing without inversion. New J Phys 2013;15:053044.

[14] Fleischhauer M, Keitel C, Su MSC. Lasing without inversion and enhancement of the index of refraction via interference of incoherent pump processes. Opt Commun 1992;87:109.

[15] Kilin SY, Kapale KT, Scully MO. Lasing without inversion: Counterintuitive population dynamics in the transient regime. Phys Rev Lett 2008;100:173601.

[16] Kozlov VV, Rostovtsev Y, Scully MO. Inducing quantum coherence via decays and incoherent pumping with application to population trapping, lasing without inversion, and quenching of spontaneous emission. Phys Rev A 2006;74:063829.

[17] Wu J-H, Gao J-Y. Phase control of light amplification without inversion in a Λ system with spontaneously generated coherence. Phys Rev A 2002;65:063807.

[18] Allen L, Padgett MJ, Babiker M. Iv the orbital angular momentum of light. Progress Opt 1999;39:291.

[19] Marrucci L, Manzo C, Paparo D. Optical spin-to-orbital angular momentum conversion in inhomogeneous anisotropic media. Phys Rev Lett 2006;96:163905.

[20] Babiker M, Power WL, Allen L. Light-induced torque on moving atoms. Phys Rev Lett 1994;73:1239.

[21] Lembessis VE, Babiker M. Light-induced torque for the generation of persistent current flow in atomic gas bose-einstein condensates. Phys Rev A 2010;82:051402.

[22] Lembessis VE, Ellinas D, Babiker M, Al-Dossary O. Atom vortex beams. Phys Rev A 2014;89:053616.

[23] Mair A, Vaziri A, Weihs G, Zeilinger A. Entanglement of the orbital angular momentum states of photons. Nature 2001;412:313.

[24] Chen Q-F, Shi B-S, Zhang Y-S, Guo G-C. Entanglement of the orbital angular momentum states of the photon pairs generated in a hot atomic ensemble. Phys Rev A 2008;78:053810.

[25] Ding D-S, Zhou Z-Y, Shi B-S, Zou X-B, Guo G-C. Linear up-conversion of orbital angular momentum. Opt Lett 2012;37:3270.

[26] Walker G, Arnold AS, Franke-Arnold S. Trans-spectral orbital angular momentum transfer via four-wave mixing in rb vapor. Phys Rev Lett 2012;108:243601.

[27] Castellucci F, Clark TW, Selyem A, Wang J, Franke-Arnold S. Atomic compass: Detecting 3d magnetic field alignment with vector vortex light. Phys Rev Lett 2021;127:233202.

[28] Tabosa JWR, Petrov DV. Optical pumping of orbital angular momentum of light in cold cesium atoms. Phys Rev Lett 1999;83:4967.

[29] He H, Friese MEJ, Heckenberg NR, Rubinsztein-Dunlop H. Direct observation of transfer of angular momentum to absorptive particles from a laser beam with a phase singularity. Phys Rev Lett 1995;75:826.

[30] Friese MEJ, Enger J, Rubinsztein-Dunlop H, Heckenberg NR. Optical angular-momentum transfer to trapped absorbing particles. Phys Rev A 1996;54:1593.

[31] Dutton Z, Ruostekoski J. Transfer and storage of vortex states in light and matter waves. Phys Rev Lett 2004;93:193602.

[32] Hamedi HR, Ruseckas J, Juzeliūas G. Exchange of optical vortices using an electromagnetically-induced-transparency–based four-wave-mixing setup. Phys Rev A 2018;98:013840.

[33] Ruseckas J, Juzeliūnas G, Öhberg P, Barnett SM. Polarization rotation of slow light with orbital angular momentum in ultracold atomic gases. Phys Rev A 2007;76:053822.

[34] Pugatch R, Shuker M, Firstenberg O, Ron A, Davidson N. Topological stability of stored optical vortices. Phys Rev Lett 2007;98:203601.

[35] Moretti D, Felinto D, Tabosa JWR. Collapses and revivals of stored orbital angular momentum of light in a cold-atom ensemble. Phys Rev A 2009;79:023825.

[36] Radwell N, Clark TW, Piccirillo B, Barnett SM, Franke-Arnold S. Spatially dependent electromagnetically induced transparency. Phys Rev Lett 2015;114:123603.

[37] Hamedi HR, Kudriasov V, Ruseckas J, Juzeliunas G. Azimuthal modulation of electromagnetically induced transparency using structured light. Opt Express 2018;26:28249.

[38] Sharma S, Dey TN. Phase-induced transparency-mediated structured-beam generation in a closed-loop tripod configuration. Phys Rev A 2017;96:033811.

[39] Zhou P, Swain S. Quantum interference in probe absorption: Narrow resonances, transparency, and gain without population inversion. Phys Rev Lett 1997;78:832.

[40] Paspalakis E, Gong S-Q, Knight PL. Spontaneous emission-induced coherent effects in absorption and dispersion of a v-type three-level atom. Opt Commun 1998;152:293.

[41] Jha PK, Ni X, Wu C, Wang Y, Zhang X. Metasurface-enabled remote quantum interference. Phys Rev Lett 2015;115:025501.

[42] Agarwal GS. Anisotropic vacuum-induced interference in decay channels. Phys Rev Lett 2000;84:5500.

[43] Li G-x, Li F-l, Zhu S-y. Quantum interference between decay channels of a three-level atom in a multilayer dielectric medium. Phys Rev A 2001;64:013819.

[44] Sun L, Jiang C. Quantum interference in a single anisotropic quantum dot near hyperbolic metamaterials. Opt Express 2016;24:7719.

[45] Hughes S, Agarwal GS. Anisotropy-induced quantum interference and population trapping between orthogonal quantum dot exciton states in semiconductor cavity systems. Phys Rev Lett 2017;118:063601.

[46] Hamedi HR, Ruseckas J, Yannopapas V, Karaoulanis D, Paspalakis E. Light-induced enhanced torque on double-v-type quantum emitters via quantum interference in spontaneous emission. Opt Laser Technol 2023;165:109550.

[47] Hamedi HR, Yannopapas V, Paspalakis E. Spatially structured optical effects in a four-level quantumsystem near a plasmonic nanostructure. Ann Phys 2021;533:2100117.

[48] Scully M, Zubairy M. Quantum optics. Cambridge: Cambridge University Press; 1997.

[49] Xu W-H, Wu J-H, Gao J-Y. Gain with and without population inversion viavacuum-induced coherence in a v-type atom withoutexternal coherent driving. J Phys B: At Mol Opt Phys 2006;39:1461.

[50] Yannopapas V, Paspalakis E, Vitanov NV. Plasmon-induced enhancement of quantum interference near metallic nanostructures. Phys Rev Lett 2009;103:063602.

[51] Li G-x, Evers J, Keitel CH. Spontaneous emission interference in negative-refractive-index waveguides. Phys Rev B 2009;80:045102.

[52] Karaoulanis D, Paspalakis E, Yannopapas V. Quantum interference near bismuth-chalcogenidemicrostructures. J Opt Soc Amer B 2021;38:3301.

[53] Kiffner M, Macovei M, Evers J, Keitel CH. Chapter 3 - vacuum-induced processes in multilevel atoms. Progress Opt 2010;55:85.

[54] Zhang S, Ni W, Kou X, Yeung MH, Sun L, Wang J, et al. Formation of gold and silver nanoparticle arrays and thin shells on mesostructured silica nanofibers. Adv Funct Mater 2007;17:3258.

[55] Liu J, Dong H, Li Y, Zhan P, Zhu M, Wang Z. A facile route to synthesis of ordered arrays of metal nanoshells with a controllable morphology. Japan J Appl Phys 2006;45:L582.

[56] Bobbert PA, Vlieger J. The polarizability of a spheroidal particle on a substrate. Physica A 1987;147:115.

[57] Wind MM, Bobbert PA, Vlieger J, Bedeaux D. The polarizability of a truncated sphere on a substrate ii. Physica A 1987;143:164.

[58] Sainidou R, Stefanou N, Modinos A. Green's function formalism for phononic crystals. Phys Rev B 2004;69:064301.

[59] Yannopapas V, Vitanov NV. Electromagnetic green's tensor and local density of states calculations for collections of spherical scatterers. Phys Rev B 2007;75:115124.

[60] Stefanou N, Yannopapas V, Modinos A. Heterostructures of photonic crystals: frequency bands and transmission coefficients. Comput Phys Comm 1998;113:49.

[61] Evangelou S, Yannopapas V, Paspalakis E. Transparency and slow light in a four-level quantum system near a plasmonic nanostructure. Phys Rev A 2012;86:053811.

[62] Wang L, Gu Y, Chen H, Zhang J-Y, Cui Y, Gerardot BD, et al. Polarized linewidth-controllable double-trapping electromagnetically induced transparency spectra in a resonant plasmon nanocavity. Sci Rep 2013;3:2879.

[63] Sukharev M, Malinovskaya SA. Stimulated raman adiabatic passage as a route to achieving optical control in plasmonics. Phys Rev A 2012;86:043406.

[64] Gu Y, Wang L, Ren P, Zhang J, Zhang T, Martin OJF, et al. Surface-plasmon-induced modification on the spontaneous emission spectrum via subwavelength-confined anisotropic purcell factor. Nano Lett 2012;12:2488.